

Contents lists available at ScienceDirect

Petroleum Science

journal homepage: www.keaipublishing.com/en/journals/petroleum-science



Original Paper

Fast simulation of EM telemetry in vertical drilling: A semi-analytical finite-element method with virtual layering technique



Hao Liang $^{\rm a}$, Chang-Chun Yin $^{\rm a,*}$, Yang Su $^{\rm a}$, Yun-He Liu $^{\rm a}$, Jun Li $^{\rm a}$, Ruo-Yun Gao $^{\rm a}$, Li-Bao Wang $^{\rm b}$

^a College of Geo-Exploration Science and Technology, Jilin University, Changchun, 130026, Jilin, China

ARTICLE INFO

Article history: Received 12 November 2024 Received in revised form 6 June 2025 Accepted 8 June 2025 Available online 14 June 2025

Edited by Jia-Jia Fei

Keywords: Electromagnetic telemetry Semi-analytical finite-element method Riccati equations High-precision integration scheme Block thomas algorithm

ABSTRACT

The electromagnetic (EM) telemetry systems, employed for real-time data transmission from the borehole and the earth surface during drilling, are widely used in measurement-while-drilling (MWD) and logging-while-drilling (LWD). Several numerical methods, including the method of moments (MoM), the electric field integral equation (EFIE) method, and the finite-element (FE) method have been developed for the simulation of EM telemetry systems. The computational process of these methods is complicated and time-consuming. To solve this problem, we introduce an axisymmetric semi-analytical FE method (SAFEM) in the cylindrical coordinate system with the virtual layering technique for rapid simulation of EM telemetry in a layered earth. The proposed method divides the computational domain into a series of homogeneous layers. For each layer, only its cross-section is discretized, and a highprecision integration method based on Riccati equations is employed for the calculation of longitudinally homogeneous sections. The block-tridiagonal structure of the global coefficient matrix enables the use of the block Thomas algorithm, facilitating the efficient simulation of EM telemetry problems in layered media. After the theoretical development, we validate the accuracy and efficiency of our algorithm through a series of numerical experiments and comparisons with the Multiphysics modeling software COMSOL. We also discussed the impact of system parameters on EM telemetry signal and demonstrated the applicability of our method by testing it on a field dataset acquired from Dezhou, Shandong Province, China.

© 2025 The Authors. Publishing services by Elsevier B.V. on behalf of KeAi Communications Co. Ltd. This is an open access article under the CC BY license (http://creativecommons.org/licenses/by/4.0/).

1. Introduction

Telemetry is a wireless, real-time communication technology that transmits data between downhole sensors and surface receivers. It is widely used in the exploration of underground resources, including minerals, oil and gas, and geothermal fields. The most commonly used telemetry techniques in measurement-while-drilling (MWD) are mud pulse telemetry and electromagnetic (EM) telemetry (Shao et al., 2017). Mud pulse telemetry has been the most widely used method since its commercialization in the 1970s (Franconi et al., 2014). However, this technique has several limitations in practical applications. Since the mud pulse

telemetry relies on pressure waves generated by a fluid hammer, a continuous flow of drilling mud is required (Li and Xu, 2023). Moreover, the mud pulse telemetry is generally unsuitable for underbalanced drilling environments and cannot be used during downhole production (Gutierrez-Estevez et al., 2013). This will lead to increased drilling costs.

In contrast, EM telemetry breaks many of the limitations in mud pulse telemetry. The EM telemetry transmits data in real-time via EM waves between the bottom-hole assembly (BHA) and surface sensors. The surface antennas measure the voltage signal between the receiver and the drilling rig (Béguin et al., 2000; Hunziker and Maurer, 2000). This technology enables the real-time acquisition of the properties of downhole formations during drilling and transmits the data back to the surface, thereby providing critical support for decision-making in terms of drilling operation optimization, efficiency, and safety. However, EM telemetry also has limitations in practical applications. For

E-mail address: yinchangchun@jlu.edu.cn (C.-C. Yin).

Peer review under the responsibility of China University of Petroleum (Beijing).

^b Huichuang Technology Co., Ltd, Linyi, 276002, Shandong, China

^{*} Corresponding author.

instance, the EM signal experiences significant attenuation in deep wells, leading to a reduction in signal strength at the earth surface. Additionally, the presence of conductive formations can further exacerbate signal attenuation (Franconi et al., 2014; Li and Xu, 2023). Therefore, in this study, we will analyze the impact of system parameters on EM telemetry signals to provide theoretical guidance for optimizing the practical application of this technology.

Early researchers conducted approximate analyses of EM telemetry using simplified models. Bhagwan and Trofimenkoff (1982) studied the low-frequency downhole-surface EM telemetry within a homogeneous medium. DeGauque and Grudzinski (1987) approximated the EM telemetry system as a quasi-static problem in a homogeneous medium and solved it using the method of moments (MoM). Xia and Chen (1993) treated the drill string as a perfect conductor and neglected the influence of drilling mud in homogeneous formations to examine the attenuation process of EM telemetry signals. Streich and Swidinsky (2023) use the MoM to analyze the effect of model discretization on the numerical results. Li et al. (2014) utilized the numerical mode matching (NMM) method to calculate EM telemetry responses in layered media for vertical wells at low frequencies and discussed the impact of system parameters on the EM telemetry signal. Yang et al. (2009) employed the electric field integral equation (EFIE) and the MoM to discretize thin casings in horizontally stratified media and calculated the current distribution on the steel casing. When using such hybrid methods to simulate EM telemetry systems, the estimation of thin-wire kernel integrations is inevitable (Wilton and Champagne, 2006). Zeng et al. (2018) combined the mixed-potential IE and MoM to simulate axial current distribution on the drill string in both vertical and horizontal wells. However, the estimation of thin-wire kernel integrations is very complex and the resulting equations system can be singular. Based on Zeng's work, Liang et al. (2020) simplified the computation of thinwire kernel integrations by using pulse functions as basis functions in the MoM.

To achieve more accurate simulations of EM telemetry systems under field-based conditions, it is necessary to develop more effective algorithms. The finite-element (FE) method demonstrates significant advantages when conducting rigorous forward simulations in complex borehole environments. The FE method can account for all features of an EM telemetry system, including the drill string, drilling fluid in the borehole, multi-layered casing, cement, and formations. However, the traditional FE method will become inefficient when simulating deep wells or when the number of underground layers is large. To simplify the model, researchers often treat the EM telemetry system as a twodimensional (2D) axisymmetric model, which only requires discretizing a plane of the underground structure in cylindrical coordinates. Poh et al. (2005) accelerated the computation by employing a hybrid axisymmetric FE combined with the surface impedance method. This implies that when they used the FE method to model the drill string, casing, drill bit, and other detailed structures, they approximated the large conductive media surrounding the drill string by a surface impedance. In recent years, Chen et al. (2011, 2017) and Chen and Zeng (2017) proposed a semi-analytical FE method (SAFEM) and applied it to the EM forward modeling in layered media for waveguide and borehole resistivity measurement. Although Chen et al. (2017) used a semianalytical finite-element method for EM telemetry simulations, their study omits the phase distribution of currents along the drill string. It is well known that the amplitude of a field component is generally easier to compute accurately than its phase. Obtaining a correct and smooth phase curve often necessitates fine mesh discretization and high computational costs. Therefore, we

propose a virtual layering technique for accurate and efficient calculation of longitudinal high-precision integration. Additionally, we optimize the coefficient matrix calculation process based on the virtual layering technique that further enhances the computational efficiency of our method.

In this study, we introduce the SAFEM to solve the simulation problem with our axisymmetric EM telemetry in the cylindrical coordinate system. The general approach of this method involves several steps. First, the layered underground is divided into subdomains with uniform geometric shapes and material distributions along the longitudinal direction. Second, the conventional FE method is used to discretize each layer's geometry along the radial direction. Finally, a high-precision integration method based on the Riccati equation is employed to compute the longitudinal integration. After assembling the coefficient matrices for each layer, the block Thomas algorithm is used to solve the system of linear equations in block tridiagonal form. The organization of this paper is as follows: we first introduce the basic theory used in our forward modeling of EM telemetry systems. After that, we validate the accuracy and efficiency of the proposed method via a series of numerical examples, followed by an analysis of how variations in system parameters affect the performance of the EM telemetry system. Finally, we demonstrate the practical applicability of the proposed method by testing on the field data acquired from Dezhou, Shandong Province, China.

2. Methodology

Fig. 1(a) schematically illustrates an operational EM telemetry system. It mainly consists of a transmitter, a drill string, and receiving electrodes/sensors. The data are transmitted in real time between the BHA and surface receivers by the current flowing along the drill string and the EM wave propagation in the surrounding formations. The red section behind the drill bit represents the EM transmitter that generates EM waves traveling through the metallic drill string and adjacent formations to the surface. The receiver, placed at the surface, is equipped with two ports: one is connected to the drill string on the rig while the other is connected to a receiving electrode positioned at a certain distance from the rig.

2.1. Governing equations

The performance of an EM telemetry system is significantly influenced by the properties of the surrounding formations. These formations are typically treated as stratified structures along the vertical axis. Consequently, the EM telemetry system in a vertical well can be modeled as an axisymmetric structure within a cylindrical coordinate system. In this model, the system parameters remain constant in the azimuthal direction, varying only radially and vertically. The system components radiating from the well center radially include the metallic drill string, the drilling fluid in the borehole, the steel casing, cement, and surrounding formations. In this study, we adopt the time-harmonic factor $e^{j\omega t}$, then the Maxwell's equations can be expressed as

$$\begin{cases}
\nabla \times \mathbf{E} = -j\omega\mu\mathbf{H} - \mathbf{M}^{\text{imp}}, \\
\nabla \times \mathbf{H} = (j\omega\varepsilon + \sigma)\mathbf{E} + \mathbf{J}^{\text{imp}}, \\
\nabla \cdot (\varepsilon\mathbf{E}) = \rho, \\
\nabla \cdot (\mu\mathbf{H}) = 0,
\end{cases} (1)$$

where ${\pmb E}$ and ${\pmb H}$ represent the electric and magnetic fields, respectively; ${\pmb J}^{\rm imp}$ represents the imposed current density; ${\pmb M}^{\rm imp}$ represents the imposed magnetic current density; ${\pmb \varepsilon}, \, {\pmb \mu}$, and ${\pmb \sigma}$ are

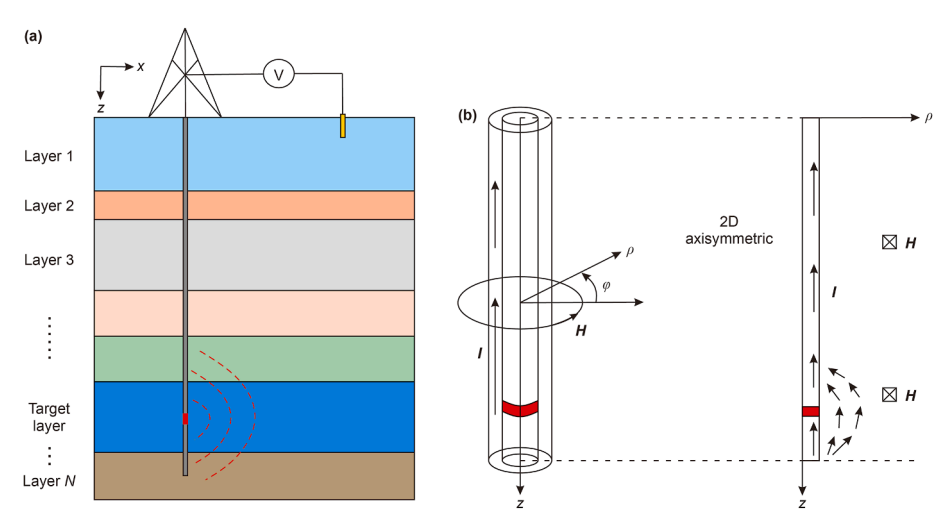


Fig. 1. (a) Schematic diagram of an EM telemetry system in a layered medium; (b) simplified model in cylindrical coordinates, where the red part represents the source, I represents the current flowing along the drill string and in the nearby formations, and H represents the magnetic field excited by the source term.

the permittivity, permeability, and conductivity of the medium, respectively; ρ denotes the charge distribution.

As mentioned above, the EM telemetry system in a vertical well can be taken as an axisymmetric structure in a cylindrical coordinate system (see Fig. 1(b)), so we only need to address a transverse magnetic (TM) problem with a magnetic current source. By taking the curl of the second term in Eq. (1) and substituting the electric field with the magnetic field, we obtain the partial differential equation for the azimuthal component \mathbf{H}_{φ} of the magnetic field in the cylindrical coordinate system as

$$\frac{1}{j\omega\varepsilon + \sigma} \left\{ \frac{\partial}{\partial\rho} \left(\frac{1}{\rho} \frac{\partial}{\partial\rho} (\rho \mathbf{H}_{\varphi}) \right) + \frac{\partial}{\partial z} \left(\frac{\partial \mathbf{H}_{\varphi}}{\partial z} \right) \right\} - j\omega\mu \mathbf{H}_{\varphi} = \mathbf{M}_{\varphi}^{imp}, \tag{2}$$

where M_{φ}^{imp} represents the imposed magnetic current density circulating the drill string that can be equivalent to an electric dipole (Li et al., 2016; Liu et al., 2024). Applying the variational principle to Eq. (2) and eliminating the azimuthal component through volume integration, we obtain

$$\prod (\mathbf{H}_{\varphi}) = \pi \int_{z_{a}}^{z_{b}} \int_{\rho_{a}}^{\rho_{b}} \frac{1}{j\omega\varepsilon + \sigma} \left\{ \left(\frac{1}{\rho} \frac{\partial}{\partial\rho} (\rho \mathbf{H}_{\varphi}) \right)^{2} + \left(\frac{\partial \mathbf{H}_{\varphi}}{\partial z} \right)^{2} \right\} \rho d\rho dz$$

$$- \pi \int_{z_{a}}^{z_{b}} \int_{\rho_{a}}^{\rho_{b}} j\omega\mu \mathbf{H}_{\varphi}^{2} \rho d\rho dz - 2\pi \int_{z_{a}}^{z_{b}} \int_{\rho_{a}}^{\rho_{b}} \mathbf{M}_{\varphi}^{imp} \mathbf{H}_{\varphi} \rho d\rho dz,$$
(3)

where z_a , z_b , ρ_a , and ρ_b define the computational domain in the cylindrical system for the EM telemetry system. From Ampere's law $\oint_I \mathbf{H} \cdot \mathrm{d}l = \mathbf{I}$, we define $\mathbf{I} = 2\pi \rho \mathbf{H}_{\varphi}$ as the current flowing along the drill string. Then, the variational form based on this current is given by

$$\prod(\mathbf{I}) = \frac{1}{4\pi} \int_{z_a}^{z_b} \int_{\rho_a}^{\rho_b} \frac{1}{j\omega\varepsilon + \sigma} \left\{ \frac{1}{\rho} \left(\frac{\partial \mathbf{I}}{\partial \rho} \right)^2 + \frac{1}{\rho} \left(\frac{\partial \mathbf{I}}{\partial z} \right)^2 \right\} d\rho dz
- \frac{1}{4\pi} \int_{z_a}^{z_b} \int_{\rho_a}^{\rho_b} \frac{1}{\rho} j\omega \mu \mathbf{I}^2 d\rho dz - \int_{z_a}^{z_b} \int_{\rho_a}^{\rho_b} \mathbf{M}_{\varphi}^{imp} \mathbf{I} d\rho dz.$$
(4)

These variational forms can be discretized using the conventional two-dimensional FE method. However, the FE method will become inefficient when dealing with large computational domains, such as deep wells or multilayered geological structures. In

this study, we employ the SAFEM to solve this axisymmetric EM problem. Considering the geometric characteristics of the EM telemetry system, we divide the computational domain into a series of vertically uniform layered structures. When applying SAFEM, the uniform layers along the longitudinal direction do not need to be discretized. Instead, only the radial geometry of each layer needs to be discretized using the one-dimensional FE method. After discretization, a scheme based on the Riccati equation (Chen and Zeng, 2017) is employed to calculate vertical integrations at high precision, while the computational speed and accuracy remain unaffected by the layer thickness. By converting the two-dimensional axisymmetric problem in the cylindrical system into a series of one-dimensional FE problems, our SAFEM method can significantly reduce the number of unknowns compared to the conventional FE method and thus greatly enhance computational efficiency.

2.2. Semi-analytical finite-element method

Based on the locations of layer interfaces and the transmitting sources, the computational domain can be decomposed into a series of vertically uniform layered structures, with their radial geometry and material properties distributed arbitrarily. By applying a one-dimensional FE to discretize the cross-section of each layer and leaving the vertical integrations untouched, the integration in Eq. (4) can be transformed into

$$\prod(\mathbf{I}) = \frac{1}{2} \int_{z}^{z_{b}} \left(\mathbf{I}^{\mathsf{T}} \mathbf{K}_{1} \mathbf{I} + \dot{\mathbf{I}}^{\mathsf{T}} \mathbf{K}_{2} \dot{\mathbf{I}} \right) dz, \tag{5}$$

where $\dot{\mathbf{I}} = \partial \mathbf{I}/\partial z$,

$$\mathbf{K}_{1} = \sum_{e=1}^{N} \int_{\rho_{a}}^{\rho_{b}} \frac{1}{2\pi} \left(\frac{1}{(j\omega\epsilon + \sigma)\rho} \frac{\partial \mathbf{N}_{e}}{\partial \rho} \cdot \frac{\partial \mathbf{N}_{e}^{\mathsf{T}}}{\partial \rho} - \frac{j\omega\mu}{\rho} \mathbf{N}_{e} \cdot \mathbf{N}_{e}^{\mathsf{T}} \right) \mathrm{d}\rho, \tag{6}$$

$$\mathbf{K}_{2} = \sum_{e=1}^{N} \int_{\rho_{a}}^{\rho_{b}} \frac{\mathbf{N}_{e} \cdot \mathbf{N}_{e}^{\mathrm{T}}}{2\pi \rho (j\omega \varepsilon + \sigma)} \mathrm{d}\rho, \tag{7}$$

 N_e represents the basis function for the e-th element. Any onedimensional interpolation function can be selected as the test function. In this study, we use a linear interpolation function as the test function. According to the uniqueness theorem, if the current

values at the upper and lower boundaries of the region are known, the final result of the longitudinal integration in Eq. (5) will be a quadratic function based on $I_a = I|_{z=z_n}, I_b = I|_{z=z_b}$, so that we have

$$\prod (\mathbf{I}_a, \mathbf{I}_b) = \frac{1}{2} \mathbf{I}_a^{\mathsf{T}} \mathbf{K}_{aa} \mathbf{I}_a + \mathbf{I}_b^{\mathsf{T}} \mathbf{K}_{ba} \mathbf{I}_a + \frac{1}{2} \mathbf{I}_b^{\mathsf{T}} \mathbf{K}_{bb} \mathbf{I}_b, \tag{8}$$

where the matrices \mathbf{K}_{aa} , \mathbf{K}_{ba} , and \mathbf{K}_{bb} can be computed using a numerical integration algorithm for the longitudinal integration in Eq. (5). However, ensuring the accuracy of numerical integration can be very challenging, while insufficient precision may limit the effectiveness of SAFEM in handling longitudinally uniform layered structures, and ultimately compromise the accuracy of the method. A high-precision integration scheme based on the Riccati equation can be employed to solve the longitudinal integration and achieve computational accuracy close to the rounding error of double-precision floating-point arithmetic. The detailed procedures for solving the matrices \mathbf{K}_{aa} , \mathbf{K}_{ba} , and \mathbf{K}_{bb} can be found in Appendix A.

2.3. Virtual layering technique and block Thomas algorithm

After obtaining the integration for the vertically uniform regions using the high-precision integration method, the coefficient matrix for the current layer is given by

$$\mathbf{K} = \begin{bmatrix} \mathbf{K}_{aa} & \mathbf{K}_{ab} \\ \mathbf{K}_{ba} & \mathbf{K}_{bb} \end{bmatrix}, \mathbf{K}_{ab} = \mathbf{K}_{ba}^{\mathrm{T}}, \tag{9}$$

once the coefficient matrix for each layer is obtained, we can assemble these matrices to form a global coefficient matrix. The source terms are then added to the corresponding positions on the right-hand side. By solving this large linear equation system, we can obtain the responses for the EM telemetry system. The global coefficient matrix derived from SAFEM takes the form of a block tridiagonal matrix, i.e.

$$\begin{bmatrix} \mathbf{B}_{1} & \mathbf{C}_{1} & \mathbf{0} & \cdots & \mathbf{0} \\ \mathbf{A}_{2} & \mathbf{B}_{2} & \mathbf{C}_{2} & \ddots & \vdots \\ \mathbf{0} & \mathbf{A}_{3} & \mathbf{B}_{3} & \ddots & \mathbf{0} \\ \vdots & \ddots & \ddots & \ddots & \mathbf{C}_{N-1} \\ \mathbf{0} & \cdots & \mathbf{0} & \mathbf{A}_{N} & \mathbf{B}_{N} \end{bmatrix} \begin{bmatrix} \mathbf{I}_{1} \\ \mathbf{I}_{2} \\ \vdots \\ \mathbf{I}_{N} \end{bmatrix} = \begin{bmatrix} \mathbf{b}_{1} \\ \mathbf{b}_{2} \\ \vdots \\ \mathbf{b}_{N} \end{bmatrix},$$
(10)

where $\mathbf{A}_i = \mathbf{K}_{ba}^{(i-1)}$, $\mathbf{B}_i = \mathbf{K}_{aa}^{(i)} + \mathbf{K}_{bb}^{(i-1)}$, and $\mathbf{C}_i = \mathbf{K}_{ab}^{(i)}$, \mathbf{I}_i and \mathbf{b}_i represent the discretized current vector and discretized excitation for the *i*-th interface, respectively.

Since the coefficient matrix in Eq. (10) has a special form, it can be solved by the MUMPS or PARDISO direct solvers based on the LU decomposition. However, the block Thomas algorithm (Chen et al., 2011; Meurant, 1992) can accelerate the overall solution process. The block Thomas algorithm is a specialized form of the Thomas algorithm designed for solving equations systems with tridiagonal matrices, and its computational cost increases linearly with the number of layers. Combining the SAFEM with the block Thomas algorithm we can significantly enhance the efficiency of our forward modeling of multi-layer EM telemetry systems.

In the simulation of the EM telemetry system, achieving a precise representation of the current flowing along the drill string requires fine discretization in the vertical direction, rather than relying solely on the actual subsurface layers to form the final linear equations. To address this, we propose the virtual layering technique to optimize the computational process. As illustrated in Fig. 2, by considering actual and required stratification for the simulation, our approach enables more flexible discretization of the vertical layers. For example, for layers far from the source, a larger thickness Δd is used, while for layers close to the source, a

smaller thickness Δd_1 is used. Although the entire system is divided into n-1 layers during the simulation, only the system parameters of N-1 layers differ. Thus, we only need to compute the coefficient matrix for a virtual layer of thickness Δd within each actual layer, and then assign this matrix to other virtual layers within the same actual layer. For virtual layers with varying thicknesses, we simply identify the corresponding actual layer and recalculate the coefficient matrix for the specific layer thickness. The pseudocode for this process is outlined below.

Algorithm 1. Global matrix calculation and block Thomas solver in SAFEM

```
Stage 1 Calculate the coefficient matrix under true stratification:
for i = 1: N do
  calculate K_1(i), K_2(i) based on Eqs. (6) and (7)
  use high-precision integration scheme to calculate matrix \mathbf{K}_{\text{true}}(i) in Eq.
  (9) with a thickness of \Delta d
Stage 2 Calculate the coefficient matrix under virtual stratification:
for j = 1: n do
   if z_{j+1} - z_j = \Delta d then
     if z_i < z_j < z_{i+1} then K(j) = K_{\text{true}}(i)
      end if
   else
     repeat stage 1 with a thickness of \Delta d_1
   end if
end for
Stage 3 Solve the linear equations system using the block Thomas
    algorithm:
C'_1 = B_1^{-1} C_1

b'_1 = B_1^{-1} I_1
for i = 2: n do
   \boldsymbol{C}_i = (\boldsymbol{B}_i - \boldsymbol{A}_i \boldsymbol{C}_{i-1})^{-1} \boldsymbol{C}_i
  \boldsymbol{b}'_i = (\boldsymbol{B}_i - \boldsymbol{A}_i \boldsymbol{C}'_{i-1})^{-1} (\dot{\boldsymbol{b}}_i - \boldsymbol{A}_i \boldsymbol{b}'_{i-1})
end for
I_n = b'_n
for i = n-1: -1: 2 do
  I_i = b'_i - C'_i I_{i+1}
end for
```

3. Numerical experiments

3.1. Algorithm validation

We first validate the effectiveness of the proposed method using a model of an EM telemetry system in a layered medium. The model consists of four layers: the first is the air, while the interfaces of the remaining three layers are located at z = 400 m and z = 700 m, respectively. The conductivities from top to bottom layer are 10^{-8} , 0.5, 0.1, and 0.05 S/m, respectively. The drill string has a length of 1000 m and a radius of 0.127 m, with 1 V voltage source placed at z = 960 m and an operating frequency of 5 Hz. Fig. 3 shows the magnitude and phase of the current flowing along the drill string. To investigate the impact of the drill string conductivity on system performance, we consider two cases of a perfectly conductive drill string (a perfect electric conductor-PEC) and a drill string with a finite conductivity of 10⁵ S/m and compare our results with those from COMSOL. In this example, each virtual layer has a thickness of $\Delta d = 20$ m. From Fig. 3, we can see that our results agree well with COMSOL, with a maximum relative error in amplitude of about 3% and a maximum absolute error in phase of 2°. The current in higher-conductivity layers decays more rapidly. This occurs because the current injected into high-conductivity layers experiences significant attenuation along the drill string. Moreover, the conductivity of the drill string can significantly affect the rate of current attenuation. As shown in the figure, the lower the drill string conductivity, the faster the current

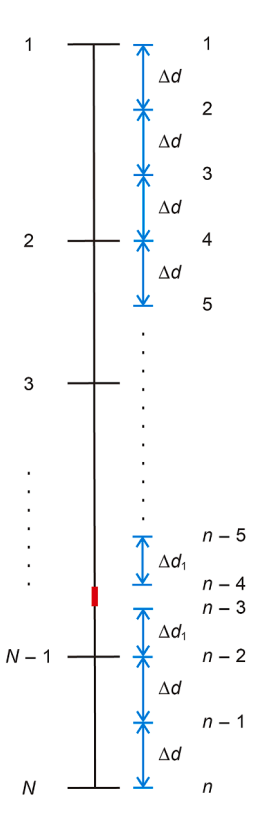


Fig. 2. Schematic diagram of a layered structure for EM telemetry system. On the left side is the real stratification in the subsurface with a total of N interfaces; on the right side is the virtual stratification with a finely discretized vertical layering, consisting of n interfaces. The red line indicates the location of the imposed source. For regular layers, the thickness is assumed to be Δd , while for layers closer to the source, a smaller thickness Δd_1 is used.

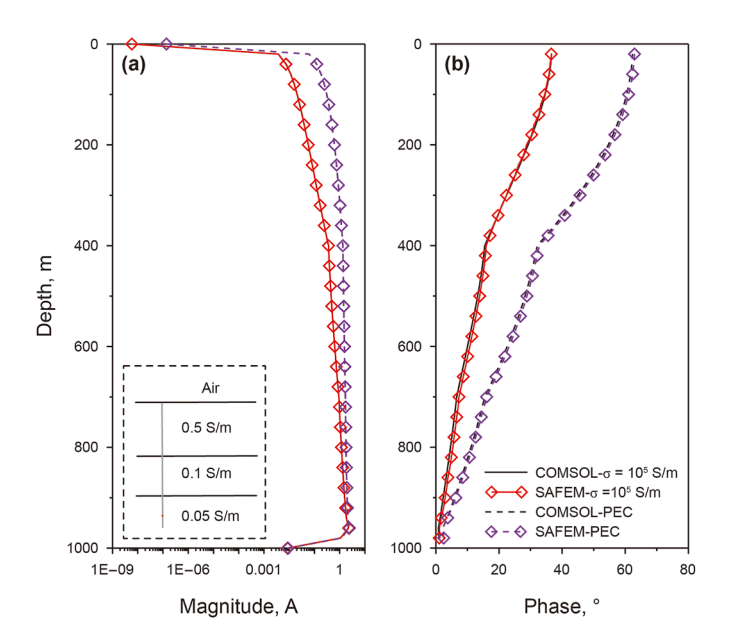


Fig. 3. Current distribution along the drill string. (a) Magnitude of the current, (b) phase of the current. The black lines represent the results from COMSOL, while the red and purple lines represent the results from the proposed method. The dashed lines reveal the current distribution when the drill string is taken as a PEC, while the solid lines reveal the current distribution when the drill string has a limited conductivity of 10^5 S/m.

Table 1Computational costs of COMSOL and SAFEM for example 1. The total time in the last two rows is the sum of the time for calculating the system matrix and solving the equations.

Method	Number of unknowns	Memory cost	CPU time
COMSOL	19,924,946	50.36 GB	508 s
SAFEM (Thomas)	53×321	800 MB	(11.3+2.9) s
SAFEM (LU)	53×321	5 GB	(11.3+15.3) s

attenuates along the string. Therefore, the impact of drill string conductivity should be taken into account in future simulations of EM telemetry systems. Table 1 compares the cost for the calculation of EM telemetry responses in vertical wells for both methods. For a fair comparison, we discretized the 2D model in a cylindrical system using COMSOL, while SAFEM used only 320 grids to discretize the interface of each layer. As we assume a total of 52 virtual layers, the number of unknowns is 53×321 (321 nodes). Table 1 illustrates that SAFEM is 35 times faster than COMSOL; while it consumes approximately 60 times less memory than COMSOL; COMSOL creates about 1000 times DOFs of SAFEM.

We further analyze the memory and time consumption of SAFEM using different solution methods. Since SAFEM discretizes models with fewer unknowns, we use the LU decomposition taken from the Intel Math Kernel Library (MKL) and the block Thomas method. Table 1 shows that, despite the parallel computation in the MKL functions, the block Thomas algorithm requires less memory and time than the LU decomposition. In dealing with deep well problems, which involve more virtual layers and unknowns, the computational time of LU decomposition increases exponentially, while the computational time of block Thomas algorithm increases only linearly. This means that combined with the block Thomas algorithm, our method can significantly reduce memory consumption and computational time.

To further validate the effectiveness of our SAFEM method, we design a more complex model with varied system parameters. Fig. 4 shows the EM telemetry system in a borehole with a uniform formation conductivity of 1 S/m. The drill string has a length of 1524 m and a radius of 0.127 m. The radius of the borehole is 0.1524 m. The length of the casing and cement is 914.4 m. The conductivity of the drilling fluid is 1 S/m and the conductivities of the drill string and casing are 2×10^6 S/m. A 1 V magnetic current source is positioned at 1463.04 m, operating at a frequency of 5 Hz. Due to large variations in the cement conductivity in different states, we select two sets of parameters with relatively high and low conductivities for the cement to explore their impact on the EM telemetry system. The virtual layer has a thickness of $\Delta d = 30.48$ m. Fig. 5 shows the calculation results of the current magnitude and phase along the drill string. The current magnitude decreases with distance from the source, as part of the current is injected into the surrounding conductive formations when flowing along the drill string. Additionally, the decay of the current above the gray line is slower, which is due to the presence of the casing that shields the current from flowing into the nearby formations. As the cement conductivity decreases, the current attenuation slows down, and the phase shows noticeable changes. Compared to the high-conductivity case, the impact of the cement conductivity becomes more apparent at 914.4 m on the phase curve. This indicates that the EM telemetry system is highly sensitive to changes in the conductivity of surrounding media. It is crucial to rigorously consider the effects of system parameters during simulations. A comparison of the computational costs of SAFEM and COMSOL is shown in Table 2. Another advantage of SAFEM, as

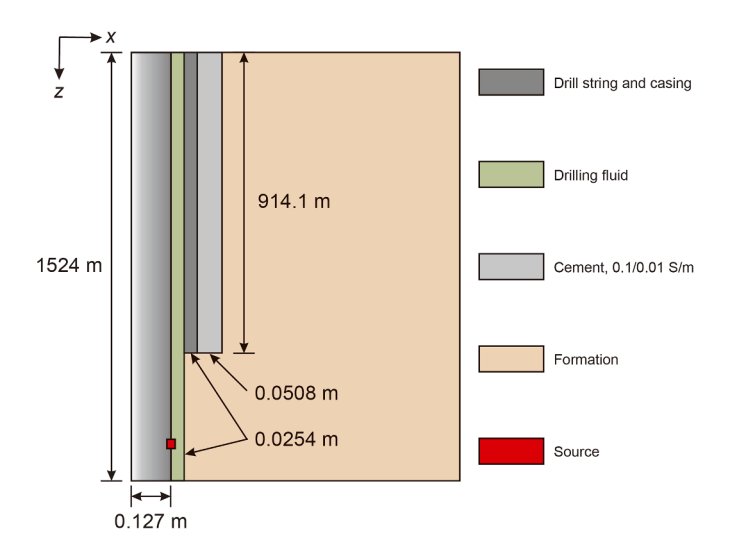


Fig. 4. Schematic diagram of an EM telemetry model that considers the actual wellbore environment. The system parameters are shown in the legend on the right side, with the red area representing the location of the imposed source.

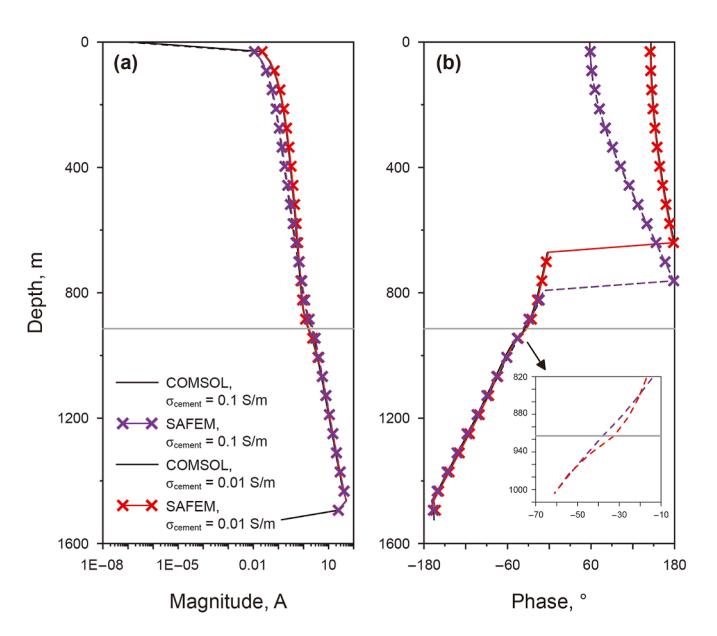


Fig. 5. Distribution of the current magnitude and phase along the drill string in complex media. The dashed lines show the responses with a cement conductivity of 0.1 S/m, while the solid lines show the responses with a cement conductivity of 0.01 S/m. The gray lines show the location at the depth of 914.4 m which marks the end of the casing and cement.

Table 2Costs of COMSOL and SAFEM methods for Example 2. The total time in the last two rows is the sum of the time for calculating the system matrix and solving the equations.

Method	Number of unknowns	Memory cost	CPU time
COMSOL	21,335,712	54.72 GB	564 s
SAFEM (Thomas)	53×321	810 MB	(8.7+2.8) s
SAFEM (LU)	53×321	5.32 GB	(8.7+13.5) s

shown in Tables 2 and is that the calculation speed and accuracy are unaffected by layer thicknesses.

In the previous example, we primarily discuss the impact of casing and cement layers used in well cementing on telemetry

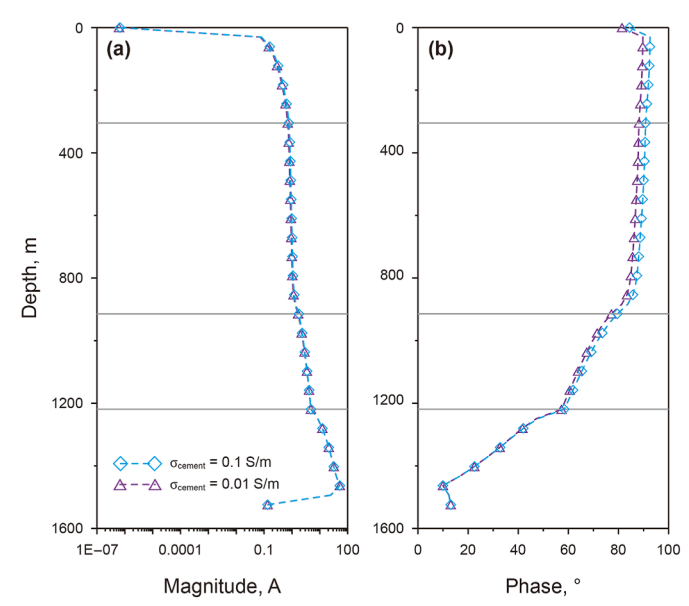


Fig. 6. Current magnitude and phase along the drill string in complex media with layered formations. The sky-blue dashed lines show the responses with a cement conductivity of 0.1 S/m, while the purple dashed lines show the responses with a cement conductivity of 0.01 S/m. The gray lines show the location of the three interfaces.

responses. To better reflect the geological diversity encountered in actual drilling, we respectively introduce three additional formation interfaces at depths of 304.8, 914.4, and 1219.2 m in the original model, dividing the formation into four layers with the conductivity of 0.05, 0.01, 0.1, and 1 S/m from top to bottom. All other parameters are consistent with the previous case. The simulation results in Fig. 6 indicate that the attenuation rate of current flowing along the drill string is proportional to the formation conductivity. In low-conductivity formations, the current attenuates slowly, whereas in high-conductivity formations, the attenuation becomes strong. This observation aligns with the conclusions drawn from Case 1. Additionally, the results also demonstrate that the cement layer above 914.4 m has a negligible effect on the current, as is observed by the amplitude curve that shows no significant variations. In the phase curve one can only see minor differences. This phenomenon can be explained. Due to the high conductivity of the surrounding formation in Case 2, a portion of the current drifts into the formation during the transmission. The casing and cement layers, acting as barriers to current flow into the formation, cause noticeable changes in both amplitude and phase. However, in the case with lower formation conductivity, the current tends to flow along the drill string and thus significantly reduces the influence of the cementing layers.

3.2. Effect of frequency

The operating frequency and formation conductivity are the two key factors affecting the signal strength of the EM telemetry system. Fig. 7 illustrates the current magnitude and phase along the drill string at various frequencies, while Fig. 8 shows the voltage signal strength detected at the surface for different frequencies, with the receiving electrode positioned at 50 m from the drilling rig. From Fig. 7(a), the current magnitude decreases as the frequency increases, and the rate of current attenuation also speeds up at higher frequencies. Additionally, Fig. 7(b) shows significant phase changes with increasing frequency. Fig. 8 indicates that when the frequency is below 10 Hz, the difference in

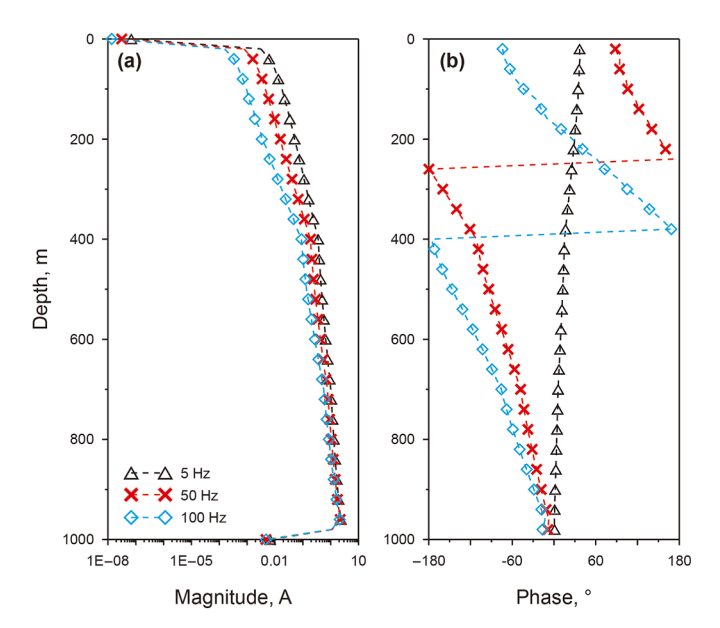


Fig. 7. The effect of operating frequency on the current flowing along the drill string. (a) Magnitude of current; (b) phase of current. The black, red, and sky-blue lines represent the results for operating frequencies of 5, 50, and 100 Hz, respectively.

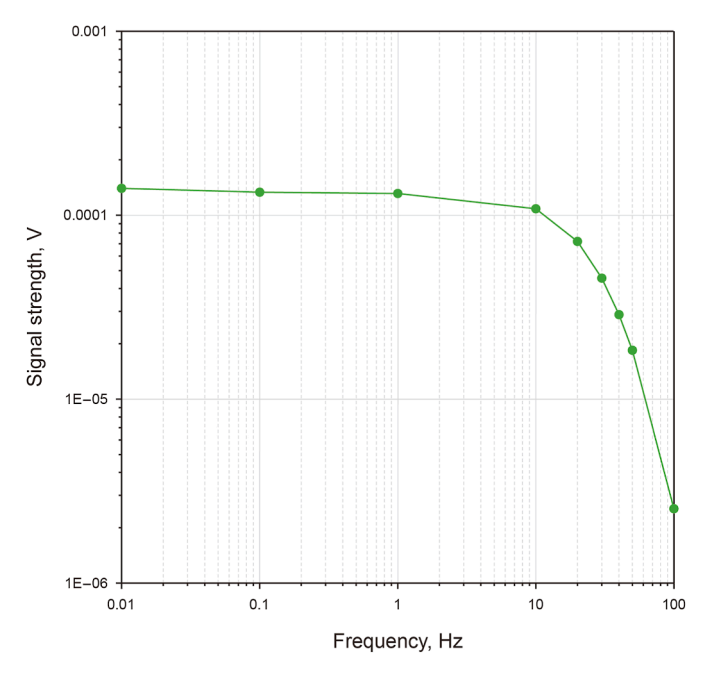


Fig. 8. Telemetry system signals at different operating frequencies.

voltage signal received at the surface is minimal. Considering both the data transmission rate and the surface signal strength, the optimal operating frequency for the EM telemetry system should be around 10 Hz. However, for deep-well measurements, the operating frequency should be reduced to ensure that the surface antenna or voltage meter can detect useful transmission signals.

3.3. Effect of layer's conductivity and thickness

To further investigate the impact of formation conductivity on the strength of EM telemetry signals, a thin layer between 520 and 580 m was added to the model in Case 1. The distribution of current along the drill string was calculated at a frequency of 10 Hz, while the conductivity of the thin layer varies from 0.01, 0.1, 1, 10, to 100 S/m. It is seen from Fig. 9(a) that the magnitude of the current in the shallower part decreases as the thin layer's conductivity increases. When the conductivity exceeds 1 S/m, a step decent of current occurs within the layer. This effect becomes more pronounced for higher conductivities. This phenomenon occurs because more current flows into the high-conductivity formation. The phase results in Fig. 9(b) also support this conclusion, showing a sudden phase shift at the location of the thin layer. Fig. 10 displays the telemetry signal received at the surface. From the figure, the signal strength decreases as the conductivity of the thin layer increases.

To further demonstrate the advantages of SAFEM, we add a 20 m-thick thin layer within the depth range of 520-540 m and assign it with high or low conductivity. As can be seen from the results in Fig. 11, when the thin layer has high conductivity, the current flowing along the drill string undergoes significant attenuation upon passing through the layer, accompanied by a sudden phase shift. In contrast, when the thin layer has a low conductivity, the current attenuation is minimal, so the phase curve exhibits a smooth variation. Moreover, the comparison of the computational cost in Table 3 highlights the efficiency advantage of SAFEM. In COMSOL, mesh refinement is required when simulating thin layers to ensure computational accuracy. This significantly increases computational cost. In contrast, the SAFEM employs a more optimized computational strategy that can effectively reduce resource consumption while maintaining high accuracy. This further underscores its superiority in handling complex formational structures.

In Fig. 12, we fix the thin layer's conductivity at 0.01 and 10 S/m and calculate the corresponding surface signals by varying the layer thickness. The results show that for a conductive layer, the surface signal strength decreases as thickness increases. Conversely, for a resistive layer, the surface signal strength increases gradually with the thickness. In summary, these findings suggest that the EM telemetry system is highly sensitive to the conductivity and thickness of the conductive formations between the downhole transmitter and the surface receiver. When a conductive layer exists between them, the telemetry signal will be significantly weakened, which is a limitation of EM telemetry compared to mud pulse telemetry.

4. Field data example

To validate the practicality of the method proposed in this study, we performed a simulation using field data from a vertical well in Dezhou, Shandong Province, China (Liang et al., 2020). The drilling depth ranges from 200 to 2000 m, with a 1.4 A current source located 100 m behind the drill bit. The operating frequency is 10 Hz, and the ground receiver is approximately 50 m away from the rig. The current source moves between 350 and 1000 m, so the drill string length varies from 450 to 1100 m. The radius of the drilling string is 0.5 m. Fig. 14(a) shows the resistivity model derived from the logging results shown in Fig. 13. It is seen from Fig. 14(b) that the simulation results obtained by SAFEM match well the trend of the field data in the mid-to-deep region. It is worth noting that, in practical applications, the results of numerical simulations and actual measurements can be influenced by many uncertainties. For instance, the surface resistivity distribution can fluctuate significantly due to changes in temperature and moisture. Additionally, borehole effects can substantially influence surface-detected signals. Consequently, the discrepancies between numerical simulation results and the measurements are

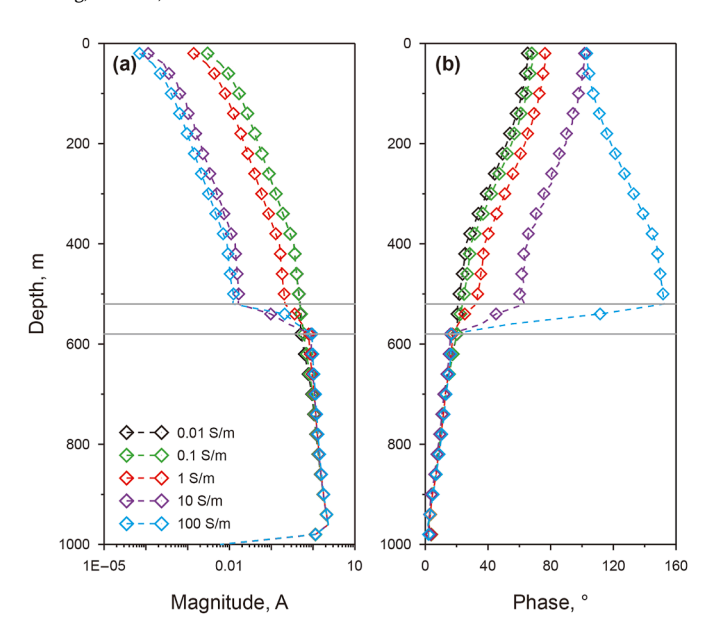


Fig. 9. Effect of thin layer conductivity on current flowing along the drill string. (a) Magnitude of the current; (b) phase of the current. The black, green, red, purple, and sky-blue lines represent the results for conductivities of 0.01, 0.1, 1, 10, and 100 S/m, respectively. The gray lines at depths of 520 and 580 m indicate the upper and lower boundaries of the thin layer.

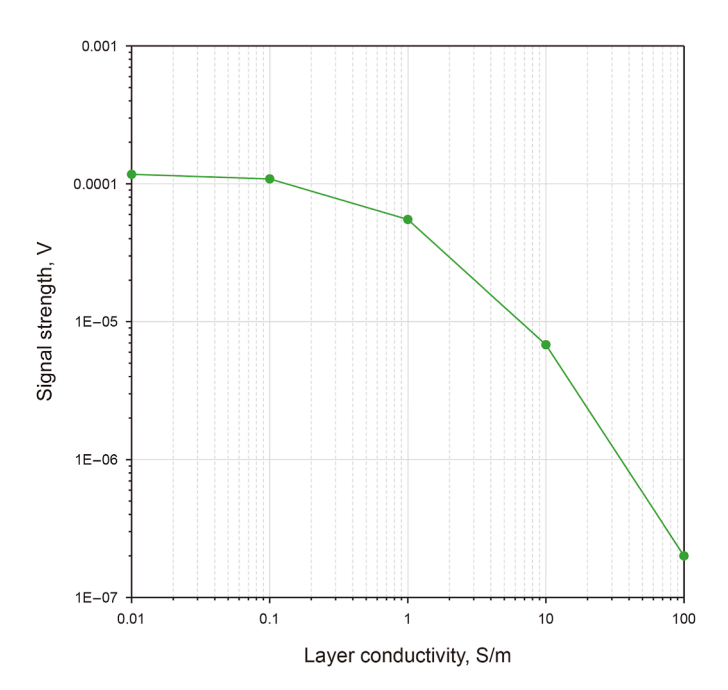


Fig. 10. Telemetry system signal under different thin layer conductivities.

unavoidable. Nevertheless, our method demonstrates good efficiency and reasonable accuracy in this field examples.

5. Conclusion

We have successfully developed an efficient and accurate simulation algorithm for axisymmetric EM telemetry systems in vertical wells using the SAFEM in cylindrical systems. By adopting the virtual layering technique, we further improve the computational efficiency of SAFEM. Due to the special structure of the coefficient matrix formed by this method, we introduce the block

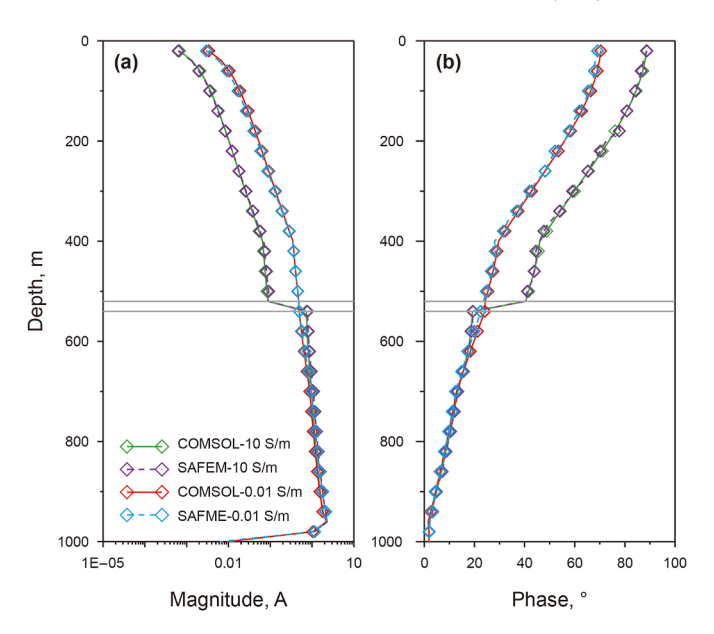


Fig. 11. The current flowing along the drill string with a 20 m thin layer. (a) Magnitude of the current; (b) phase of the current. The green and red lines represent the results for conductivities of 10 and 0.01 S/m using COMSOL, while the purple and skyblue dashed lines represent the results for conductivities of 10 and 0.01 S/m using SAFEM. The gray lines at depths of 520 and 540 m indicate the upper and lower boundaries of the thin layer.

Table 3Costs of COMSOL and SAFEM for the thin layer with a thickness of 20 m. The total time in the last two rows is the sum of the time for calculating the system matrix and solving the equations.

Method	Number of unknowns	Memory cost	CPU time
COMSOL	20,641,708	52.41 GB	532 s
SAFEM (Thomas)	53×321	841 MB	(13.0+3.3) s
SAFEM (LU)	53×321	5.35 GB	(13.0+13.5) s

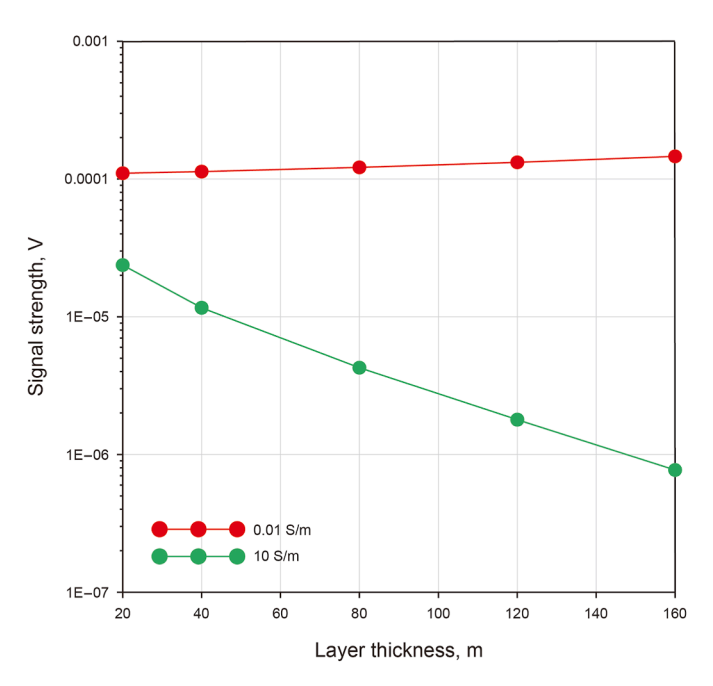


Fig. 12. Telemetry system signal at varying thicknesses with a thin layer of conductivity of 0.01 and 10 S/m, respectively.

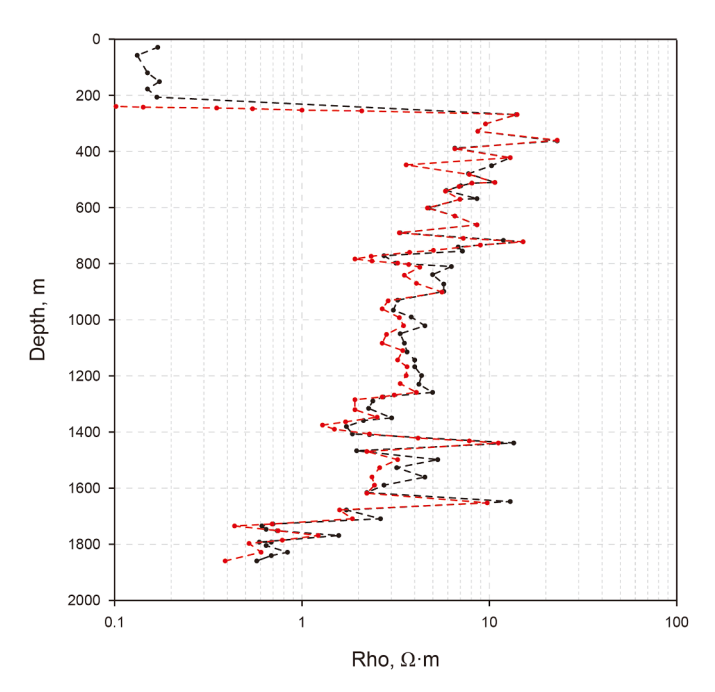


Fig. 13. Logging curves of the field data example in Shandong, China. The black line is the lateral logging curve and the red line is the normal logging curve.

Thomas algorithm for solving the linear equations system. The numerical experiments have shown that in this way the computational efficiency is largely enhanced and the memory consumption is largely reduced when comparing the software COMSOL. This makes it possible for us to handle deep well problems without significantly increasing the computational cost. The analysis of the impact of system parameters on the strength of EM telemetry signals also showed that the conductivity of the drill string, the operating frequency, and the layer conductivity could significantly impact the signal strength of the EM telemetry system. When the frequency is below 10 Hz, both the current distribution and the surface signal are nearly unaffected. However, with increasing frequency, the current distribution changes noticeably while the surface signal decreases. Moreover, the EM telemetry system is highly sensitive to well-conductive layers between the downhole source and the surface receiver. An increase in layer conductivity or thickness in such a conductive layer will weaken the signal received at the surface. The system parameters analyzed in this study aim to provide guidance for the design and execution of the EM telemetry surveys.

CRediT authorship contribution statement

Hao Liang: Writing – review & editing, Writing – original draft, Software, Methodology, Formal analysis, Conceptualization. **Chang-Chun Yin:** Writing – review & editing, Validation,

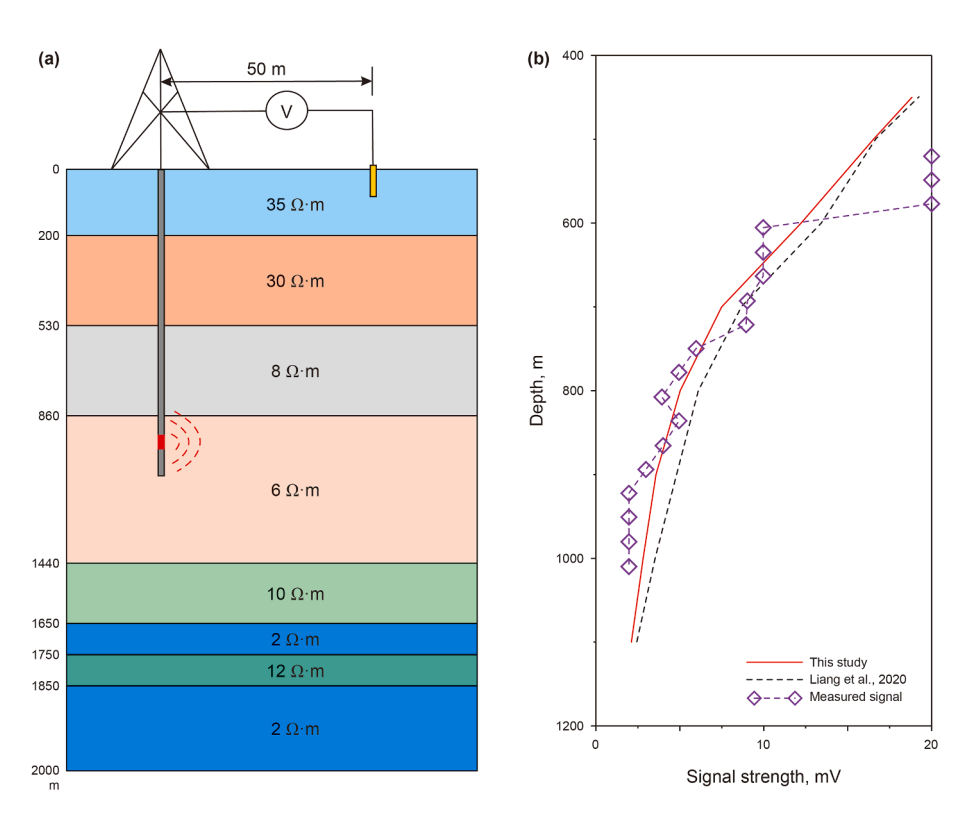


Fig. 14. Simulating the field data from Shandong, China. (a) Resistivity model used for the simulation; (b) magnitude of the telemetry signal received at the surface 50 m from the drilling rig. The red line represents the simulation results using our SAFEM method, the black dashed line represents the simulation results from Liang et al. (2020), and the purple dashed line represents the survey signals.

Supervision, Funding acquisition, Formal analysis. **Yang Su:** Investigation, Funding acquisition. **Yun-He Liu:** Validation, Investigation, Conceptualization. **Jun Li:** Validation, Formal analysis. **Ruo-Yun Gao:** Investigation, Data curation. **Li-Bao Wang:** Investigation, Funding acquisition.

Declaration of competing interest

The authors declare that they have no known competing financial interests or personal relationships that could have appeared to influence the work reported in this paper.

Acknowledgments

This paper is financially supported by the Major Research Project on Scientific Instrument Development of the National Natural Science Foundation of China (42327901) and National Natural Science Foundation of China (42030806, 42074120, 41904104, 423B2405).

Appendix A

Here, we provide a high-precision integration scheme for solving the longitudinal integration in Eq. (8). This scheme, based on the Riccati equation, allows for the efficient calculation of the longitudinal integrals in Eq. (8). As demonstrated by Zhong (2004, 2006), the system matrices K_{aa} , K_{ba} , and K_{bb} satisfy the following relationships, i.e.

$$\begin{cases} \mathbf{K}_{aa} = -\mathbf{Q} + \mathbf{F}^{\mathrm{T}} \mathbf{G}^{-1} \mathbf{F} \\ \mathbf{K}_{ba} = -\mathbf{G}^{-1} \mathbf{F} \\ \mathbf{K}_{bb} = \mathbf{G}^{-1} \end{cases}, \tag{A-1}$$

where the matrices ${\bf Q}$, ${\bf F}$, and ${\bf G}$ are solutions to a set of Riccati equations, i.e.

$$\begin{cases} dF/d\eta = -GBF = FDQ \\ dG/d\eta = D - GBG = FDF^{T}, \\ dQ/d\eta = -FBF = QDQ - B \end{cases}$$
(A-2)

with the initial conditions of

$$\begin{cases}
\mathbf{Q}|_{\eta \to 0} = \mathbf{0} \\
\mathbf{G}|_{\eta \to 0} = \mathbf{0} \\
\mathbf{F}|_{\eta \to 0} = \mathbf{I}
\end{cases}$$
(A-3)

where $\mathbf{B} = \mathbf{K}_1$, $\mathbf{D} = \mathbf{K}_2^{-1}$. \mathbf{K}_1 and \mathbf{K}_2 can be calculated using Eq. (6) and Eq. (7), respectively. $\eta = z_b - z_a$ represents the thickness of the current layer, while $\mathbf{0}$ and \mathbf{I} denote the zero and unit matrix with the same dimensions as \mathbf{K}_1 and \mathbf{K}_2 .

To implement the high-precision integration scheme based on the Riccati equation, there are two key points: one is to divide the integration interval based on the 2^N division method, while the other is to avoid rounding errors during the computation. Thus, we first divide the integration interval η into 2^N segments, i.e.

$$\tau = \frac{\eta}{2^N},\tag{A-4}$$

where N is a positive integer, and typically N=20 is sufficient to achieve an integration accuracy that meets the double precision defined by a computer. This means that even if the layer thickness is 100 times as the wavelength, the length of each integration interval τ will still be less than 1/10,000 of the wavelength. Within this sufficiently small interval τ , we can calculate the matrices \mathbf{Q} , \mathbf{F} , and \mathbf{G} using the Taylor series expansion, namely

$$\begin{cases}
\mathbf{F}(\tau) = \mathbf{I} + \mathbf{F}(\tau) \\
\mathbf{F}(\tau) = \boldsymbol{\varphi}_{1}\tau + \boldsymbol{\varphi}_{2}\tau^{2} + \boldsymbol{\varphi}_{3}\tau^{3} + \boldsymbol{\varphi}_{4}\tau^{4} + O(\tau^{5}) \\
\mathbf{G}(\tau) = \boldsymbol{\gamma}_{1}\tau + \boldsymbol{\gamma}_{2}\tau^{2} + \boldsymbol{\gamma}_{3}\tau^{3} + \boldsymbol{\gamma}_{4}\tau^{4} + O(\tau^{5}) \\
\mathbf{Q}(\tau) = \boldsymbol{\theta}_{1}\tau + \boldsymbol{\theta}_{2}\tau^{2} + \boldsymbol{\theta}_{3}\tau^{3} + \boldsymbol{\theta}_{4}\tau^{4} + O(\tau^{5})
\end{cases}$$
(A-5)

where the matrices φ , γ , and θ have the same dimensions as the matrices \mathbf{Q} , \mathbf{F} , and \mathbf{G} . Since the integration interval τ is extremely small, the terms of higher-order error $O(\tau^5)$ in the Taylor expansion can be neglected without losing accuracy. By comparing Eq. (A-5) with the Riccati Eq. (A-2), we obtain the expressions for the matrices φ , γ , and θ , i.e.

$$\begin{cases} \gamma_1 = \mathbf{D} \\ \gamma_2 = \mathbf{0} \\ \gamma_3 = -\gamma_1 \mathbf{B} \gamma_1 / 3 \\ \gamma_4 = (-\gamma_2 \mathbf{B} \gamma_1 - \gamma_1 \mathbf{B} \gamma_2) / 4 \end{cases}$$
(A-6)

$$\begin{cases} \boldsymbol{\varphi}_{1} = \mathbf{0} \\ \boldsymbol{\varphi}_{2} = -\gamma_{1} \mathbf{B} / 2 \\ \boldsymbol{\varphi}_{3} = (-\gamma_{2} \mathbf{B} - \gamma_{1} \mathbf{B} \boldsymbol{\varphi}_{1}) / 3 \\ \boldsymbol{\varphi}_{4} = (-\gamma_{3} \mathbf{B} - \gamma_{2} \mathbf{B} \boldsymbol{\varphi}_{1} - \gamma_{1} \mathbf{B} \boldsymbol{\varphi}_{2}) / 4 \end{cases}$$
(A-7)

$$\begin{cases} \boldsymbol{\theta}_{1} = -\mathbf{B} \\ \boldsymbol{\theta}_{2} = \left(-\boldsymbol{\varphi}_{1}^{\mathsf{T}}\mathbf{B} - \mathbf{B}\boldsymbol{\varphi}_{1}\right)/2 \\ \boldsymbol{\theta}_{3} = \left(-\boldsymbol{\varphi}_{2}^{\mathsf{T}}\mathbf{B} - \mathbf{B}\boldsymbol{\varphi}_{2} - \boldsymbol{\varphi}_{1}^{\mathsf{T}}\mathbf{B}\boldsymbol{\varphi}_{1}\right)/3 \\ \boldsymbol{\theta}_{4} = \left(-\boldsymbol{\varphi}_{3}^{\mathsf{T}}\mathbf{B} - \mathbf{B}\boldsymbol{\varphi}_{3} - \boldsymbol{\varphi}_{2}^{\mathsf{T}}\mathbf{B}\boldsymbol{\varphi}_{1} - \boldsymbol{\varphi}_{1}^{\mathsf{T}}\mathbf{B}\boldsymbol{\varphi}_{2}\right)/4 \end{cases}$$
(A-8)

Substituting Eq. (A-6) to Eq. (A-8) into Eq. (A-5), we obtain the matrix values within an integration interval τ . Using the segment merging algorithm, the matrix for the interval 2τ is then given by

$$\begin{cases}
\mathbf{G}(2\tau) = \mathbf{G}(\tau) + \mathbf{F}(\tau) \left[\mathbf{G}(\tau)^{-1} + \mathbf{Q}(\tau) \right]^{-1} \mathbf{F}(\tau)^{\mathrm{T}} \\
\mathbf{F}'(2\tau) = \mathbf{F}'(\tau) [\mathbf{I} + \mathbf{G}(\tau) \mathbf{Q}(\tau)]^{-1} \mathbf{F}'(\tau) \\
+ [(\mathbf{F}'(\tau) - \mathbf{G}(\tau) \mathbf{Q}(\tau)/2)] [\mathbf{I} + \mathbf{G}(\tau) \mathbf{Q}(\tau)]^{-1} \\
+ [\mathbf{I} + \mathbf{G}(\tau) \mathbf{Q}(\tau)]^{-1} [(\mathbf{F}'(\tau) - \mathbf{G}(\tau) \mathbf{Q}(\tau)/2)] \\
\mathbf{Q}(2\tau) = \mathbf{Q}(\tau) + \mathbf{F}(\tau)^{\mathrm{T}} \left[\mathbf{Q}(\tau)^{-1} + \mathbf{G}(\tau) \right]^{-1} \mathbf{F}(\tau)
\end{cases} (A-9)$$

It is important to note that during the calculation process, we only compute and store the increment of matrix \mathbf{F} , denoted by \mathbf{F} . Since the initial matrix \mathbf{F} is an identity one, the increment \mathbf{F} is much smaller than \mathbf{I} . If we directly add this increment to the matrix \mathbf{F} , the increment \mathbf{F} may be ignored due to rounding errors in the computer. By iterating Eq. (A-9) N times, we can accurately calculate the matrices \mathbf{Q} , \mathbf{F} , and \mathbf{G} over the entire integration interval η . Substituting these matrices into Eq. (A-1) we will be able to obtain the system matrices \mathbf{K}_{aa} , \mathbf{K}_{ba} , and \mathbf{K}_{bb} for the current layer.

References

Béguin, P., Benimeli, D., Boyd, A., Dubourg, I., Ferreira, A., McDougall, A., Rouault, G., Van Der Wal, P., 2000. Recent Progress on Formation Resistivity Measurement through Casing. SEG Technical Program Expanded Abstracts., pp. 1794–1797. https://doi.org/10.1190/1.1815773

Bhagwan, J., Trofimenkoff, F.N., 1982. Electric drill stem telemetry. IEEE Trans. Geosci. Remote Sensing GE-20 (2), 193–197. https://doi.org/10.1109/TGRS.1982.350397.

Chen, J., Zeng, S., 2017. Hybridizing semianalytical and conventional finite-element schemes for simulations of electromagnetic borehole resistivity measurement. Geophysics 82, E17–E26. https://doi.org/10.1190/geo2015-0628.1.

Chen, J., Zeng, S., Dong, Q., Huang, Y., 2017. Rapid simulation of electromagnetic telemetry using an axisymmetric semianalytical finite element method. J. Appl. Geophys. 137, 49–54. https://doi.org/10.1016/j.jappgeo.2016.12.006.

- Chen, J., Zhu, B., Zhong, W., Liu, Q.H., 2011. A semianalytical spectral element method for the analysis of 3-D layered structures. IEEE Trans. Microw. Theor. Tech. 59, 1–8. https://doi.org/10.1109/TMTT.2010.2090408.
- DeGauque, P., Grudzinski, R., 1987. Propagation of electromagnetic waves along a drillstring of finite conductivity. SPE Drill. Eng. 2, 127–134. https://doi.org/ 10.2118/12943-PA.
- Franconi, N.G., Bunger, A.P., Sejdić, E., Mickle, M.H., 2014. Wireless communication in oil and gas wells. Energ. Tech. 2, 996–1005. https://doi.org/10.1002/ente.201402067.
- Gutierrez-Estevez, M.A., Krueger, U., Krueger, K.A., Manolakis, K., Jungnickel, V., Jaksch, K., Krueger, K., Mikulla, S., Giese, R., Sohmer, M., Reich, M., 2013. Acoustic broadband communications over deep drill strings using adaptive OFDM. In: 2013 IEEE Wireless Communications and Networking Conference (WCNC), Shanghai, China, pp. 4089–4094. https://doi.org/10.1109/WCNC.2013.6555232.
- Hunziker, J., Maurer, H.M., 2000. Early results of through casing resistivity field tests. Petrophysics-The SPWLA Journal of Formation Evaluation and Reservoir Description 41 (4).
- Li, C., Xu, Z., 2023. A review of communication technologies in mud pulse telemetry systems. Electronics 12, 3930. https://doi.org/10.3390/electronics12183930.
- Li, W., Nie, Z., Sun, X., 2016. Wireless transmission of MWD and LWD signal based on guidance of metal pipes and relay of transceivers. IEEE Trans. Geosci. Rem. Sens. 54, 4855–4866. https://doi.org/10.1109/TGRS.2016.2552245.
- Li, W., Nie, Z., Sun, X., Chen, Y., 2014. Numerical modeling for excitation and coupling transmission of near field around the metal drilling pipe in lossy formation. IEEE Trans. Geosci. Rem. Sens. 52, 3862–3871. https://doi.org/ 10.1109/TGRS.2013.2277231
- Liang, P., Di, Q., Zhen, Q., Wang, R., Fayemi, O., Fu, C., Lei, D., An, Z., Fan, J., Ma, Z., Yang, L., 2020. Electromagnetic telemetry simulation in vertical drillings. Geophysics 85, E207–E219. https://doi.org/10.1190/geo2019-0568.1.

- Liu, R., Zhang, W., Chen, W., Liang, P., Liu, W., Li, X., 2024. Analysis and experimental research on the factors affecting downhole inductive electromagnetic wave wireless short-hop transmission. IEEE Trans. Geosci. Rem. Sens. 62, 1–11. https://doi.org/10.1109/TGRS.2024.3398030.
- Meurant, G., 1992. A review on the inverse of symmetric tridiagonal and block tridiagonal matrices. SIAM J. Matrix Anal. Appl. 13, 707–728. https://doi.org/10.1137/0613045.
- Poh, Kheong Vong, Rodger, D., Marshall, A., 2005. Modeling an electromagnetic telemetry system for signal transmission in oil fields. IEEE Trans. Magn. 41, 2008–2011. https://doi.org/10.1109/TMAG.2005.846272.
- Shao, J., Yan, Z., Han, S., Li, H., Gao, T., Hu, X., Wei, C., 2017. Differential signal extraction for continuous wave mud pulse telemetry. J. Petrol. Sci. Eng. 148, 127–130. https://doi.org/10.1016/j.petrol.2016.09.047.
- Streich, R., Swidinsky, A., 2023. On method-of-moments modelling of electromagnetic sources connected to metallic well casings. Geophys. J. Int. 234, 1476–1483. https://doi.org/10.1093/gji/ggad146.
- Wilton, D.R., Champagne, N.J., 2006. Evaluation and integration of the thin wire kernel. IEEE Trans. Antenn. Propag. 54, 1200–1206. https://doi.org/10.1109/ TAP.2005.872569
- Xia, M.Y., Chen, Z.Y., 1993. Attenuation predictions at extremely low frequencies for measurement-while-drilling electromagnetic telemetry system. IEEE Trans. Geosci. Rem. Sens. 31, 1222–1228. https://doi.org/10.1109/36.317441.
- Yang, W., Torres-Verdín, C., Hou, J., Zhang, Z. Ian, 2009. 1D subsurface electromagnetic fields excited by energized steel casing. Geophysics 74, E159–E180. https://doi.org/10.1190/1.3131382.
- Zeng, S., Li, D., Wilton, D.R., Chen, J., 2018. Fast and accurate simulation of electromagnetic telemetry in deviated and horizontal drilling. J. Petrol. Sci. Eng. 166, 242–248. https://doi.org/10.1016/j.petrol.2018.03.025.
- Zhong, W., 2004. On precise integration method. J. Comput. Appl. Math. 163, 59–78. https://doi.org/10.1016/j.cam.2003.08.053.
- Zhong, W., 2006. Duality System in Applied Mechanics and Optimal Control. Springer Science & Business Media.